Gamma band directional interactions between basal forebrain and visual cortex during wake and sleep states

Jayakrishnan Nair [a], Arndt-Lukas Klaassen [a,b], Jordan Poirot [a], Alexei Vyssotski [c], Björn Rasch [b], Gregor Rainer [a,*]

[a] Visual Cognition Laboratory, Department of Medicine, University of Fribourg, Chemin du Musée 5, 1700 Fribourg, Switzerland
[b] Department of Psychology, University of Fribourg, Rue P.A. de Faucigny 2, 1700 Fribourg, Switzerland
[c] Institute of Neuroinformatics, University of Zürich/ETHZ, Winterthurerstrasse 190, 8057 Zürich, Switzerland

The basal forebrain (BF) is an important regulator of cortical excitability and responsivity to sensory stimuli, and plays a major role in wake-sleep regulation. While the impact of BF on cortical EEG or LFP signals has been extensively documented, surprisingly little is known about LFP activity within BF. Based on bilateral recordings from rats in their home cage, we describe endogenous LFP oscillations in the BF during quiet wakefulness, rapid eye movement (REM) and slow wave sleep (SWS) states. Using coherence and Granger causality methods, we characterize directional influences between BF and visual cortex (VC) during each of these states. We observed pronounced BF gamma activity particularly during wakefulness, as well as to a lesser extent during SWS and REM. During wakefulness, this BF gamma activity exerted a directional influence on VC that was associated with cortical excitation. During SWS but not REM, there was also a robust directional gamma band influence of BF on VC. In all three states, directional influence in the gamma band was only present in BF to VC direction and tended to be regulated specifically within each brain hemisphere. Locality of gamma band LFPs to the BF was confirmed by demonstration of phase locking of local spiking activity to the gamma cycle. We report novel aspects of endogenous BF LFP oscillations and their relationship to cortical LFP signals during sleep and wakefulness. We link our findings to known aspects of GABAergic BF networks that likely underlie gamma band LFP activations, and show that the Granger causality analyses can faithfully recapitulate many known attributes of these networks.

1. Introduction

The BF is an important regulator of cortical activity (Semba, 2000; Jones, 2003; Zaborszky and Duque, 2003; Lin et al., 2015). Thus, lesions of the BF result in abnormalities of cortical EEG or LFP signals. Increases of delta (1–4 Hz) activity (Buzsaki et al., 1988; Kaur et al., 2008; Fuller et al., 2011) as well as reductions in gamma (30–90 Hz) activity (Berntson et al., 2002) have been reported following BF lesions. Since the cholinergic neurons of the BF are the major source of Acetylcholine to neocortex, much work has focused on the functional role of this projection system. However, BF contains cholinergic, glutamatergic and GABAergic corticopetal projection systems, and considerable effort has been made in attempting to link these specific projection systems to

modulations of the cortical EEG. Evidence from lesion studies suggests that selective immunotoxic lesions of the cholinergic projection system are insufficient for causing changes in cortical EEG (Kaur et al., 2008; Fuller et al., 2011). However, more extensive lesions that affect also the GABAergic corticopetal systems have been linked to enhanced delta band EEG activity and very extensive lesions induce a coma-like state with almost exclusive delta wave EEG (Fuller et al., 2011). Consistent with these findings, increased delta band EEG has also been observed following the infusion of agents that inhibit cholinergic (Cape and Jones, 1998; Toth et al., 2005; Tóth et al., 2007) or GABAergic BF neurons (Anaclet et al., 2015). These studies suggest that BF cholinergic and non-cholinergic, in particular the GABAergic neurons, operate in an ensemble manner in order to influence cortical activity.

Activation of BF has opposite effects of BF lesions on the cortical EEG. Using BF electrical microstimulation, which is thought to cause non-specific activation regardless of cell type, many studies have demonstrated suppression of delta activity and an enhance-

---

* Corresponding author at: Department of Medicine, University of Fribourg, Chemin du Musée 5, CH-1700 Fribourg, Switzerland.
 E-mail address: gregor.rainer@unifr.ch (G. Rainer).

ment of higher frequency and in particular gamma oscillations (Metherate et al., 1992; McLin et al., 2002; Bhattacharyya et al., 2013). Similar excitatory effects on cortical EEG can be elicited by pharmacological activation of BF neurons, as has been demonstrated using infusion of nonspecific glutamate receptor agonists (Cape and Jones, 2000) or substances that target BF cholinergic neurons such as Neurotensin (Cape et al., 2000) or Noradrenalin (Cape and Jones, 1998). Recent findings have emphasized the importance of the GABAergic corticopetal system for initiating and sustaining EEG gamma oscillations. Accordingly, chemogenetic (Anaclet et al., 2015) or optogenetic (Kim et al., 2015) activation of GABAergic BF neurons has been shown to evoke robust cortical gamma oscillations, an effect that persists even when cholinergic BF neurons are destroyed using immunotoxic lesions (Kim et al., 2015). Indeed, previous studies demonstrating enhanced responsivity and sensitivity of visual cortical neurons following BF stimulation have already suggested a prominent role for the GABAergic corticopetal system based on the observation that the effect of BF stimulation on VC cannot be accounted for by cholinergic mechanisms alone (Bhattacharyya et al., 2012, 2013). Taken together, manipulations of BF activity have been linked to cortical EEG modulations, particularly relating to the delta and gamma frequency bands. These effects are mediated mainly by GABAergic and also by cholinergic corticopetal systems.

Recording neural activity in BF has also provided insights into how BF projections modulate the cortical EEG. Such studies have almost exclusively focused on recording the activity of single neurons, often labelled according to cell type, and linking their firing patterns to the cortical EEG (Duque et al., 2000; Manns et al., 2000a, 2000b; Hassani et al., 2009), wake/sleep regulation (Szymusiak et al., 2000; Lee et al., 2004, 2005), aspects of sensory stimulation (Lin and Nicolelis, 2008; Nguyen and Lin, 2014), and behavioral task performance (Thomson et al., 2014; Tingley et al., 2014, 2015). Convergent evidence (Zaborszky et al., 1999; Yang et al., 2014; Xu et al., 2015) indicates that BF contains multiple interconnected and heterogeneous networks, which operate as an ensemble to modulate cortical state and play distinct roles during sleep and wakefulness. It is thus quite surprising that very little is known about BF ensemble activity, as estimated by the LFP; but see (Quinn et al., 2010; Whitmore and Lin, 2016). The LFP might provide a useful window into the aggregate activation state of BF corticopetal and local networks that might be linked to specific activation patterns of these networks during REM and slow-wave sleep as well as wakefulness. In addition, simultaneous LFP recordings in BF and cortex could yield insights into the functional interactions between these regions. Methods that can reveal directionality of interactions between BF and cortex based on LFP signals might be particularly useful in this context. This can be achieved for example using autoregressive modelling or Granger causality analyses (Bressler and Seth, 2011; Seth et al., 2015), which have been used to obtain insights into local processing within brain regions (Chen et al., 2014; Plomp et al., 2014), as well as distant interactions between brain regions (Brovelli et al., 2004; Wilson et al., 2010; Kang et al., 2015) based on LFP or EEG signals.

Here we recorded bilateral LFPs from rat BF and VC, in order to comprehensively characterize BF LFPs and study functional interactions between the two brain regions. We found strong dependence of BF LFP signals on brain state. We describe spectral differences between wakefulness, REM and SWS, with gamma oscillations occurring during all states but being particularly pronounced during wakefulness. Based on coherence and Granger causality analyses, we present evidence for directional BF-cortex interactions in the gamma band during wakefulness and SWS, consistent with corticopetal modulations originating from a BF source.

2. Methods

Animals and surgery: Adult male Long Evans rats (80–120 days old, $n = 8$) were used in this study with free access to food and water. General anaesthesia was induced using a mixture of ketamine and xylazine (i.p.) and maintained using isoflurane (3.0–4.5%) in pure O_2 inhalation. We used tungsten microelectrodes of 200 μm diameter for implantation in both VC (target coordinates: 1 mm anterior and 1.5 mm ventral from lambda and 3.5 mm lateral from the midline corresponding approximately to the primary visual cortex) and BF (target coordinates Nucleus Basalis: 0.8 mm posterior from bregma, 2.8 mm lateral and 8.2 mm ventral) bilaterally. We verified based on histology for all available animals ($n = 6$) that BF recording sites were located within a 500 μm radius of the target coordinates. For VC, histological reconstruction was not possible due to the electrode track artefact, but we consider the recordings to originate from the infra-granular layers based on implantation depth during surgery. Additionally, one screw electrode placed on the midline over the cerebellum, served as both reference and ground electrode (target coordinates: 3 mm posterior from lambda). Each electrode was connected to flexible wires that were in turn connected to a 7-pin connector that was suitable for connection to a custom-made miniature neural recording device. The connector and leads were fixed and stabilized with dental cement to the animal's skull and the animals were allowed at least two weeks to recover after surgery. All experimental procedures were in compliance with European and applicable Swiss regulations.

Neural recordings: Animals were housed in 12-h dark/12-h light cycle (light on between 7:00 and 19:00). All the recording sessions were performed between 12:00 and 18:00. Recordings were performed by using a miniaturized data logger (Neurologger 2A) which has four channels for LFP recordings. Movements of the animal were registered by the Neurologger in a separate three channels through a 3-D accelerometer, providing sensitive signals related to locomotion that we used in lieu of EMG activity. The signals were recorded at a sampling rate of 1600 Hz and data were downloaded to a PC at the end of the recording session for analysis. Movement signals did not differ during SWS and REM sleep, but we did observe transient movement sensor activity around and preceding state transitions between sleep states or sleep and wakefulness. For tethered recordings, we connected the implanted electrodes to a Tucker-Davis RZ5 system using a motorized commutator, and digitized the waveforms at 22 kHz. This allowed clustering of neural spiking activity, which we used to confirm locality of gamma band LFPs in the basal forebrain in 4 animals.

Behavioral analysis: We used the cortical LFP, movement sensor data, and videographic records to manually define epochs of wakefulness, REM and SWS. Specifically we first segregated the WAKE state from the two sleep states based on the 3-D accelerometer data. Next SWS and REM sleep stages were determined by the theta (5–10 Hz)/delta (1–5 Hz) ratio extracted from the power spectrum of the LFP from VC, according to generally accepted practice (Grosmark et al., 2012; de Lavilléon et al., 2015).

Pre-processing and Spectral analysis of LFPs: The LFP data were down-sampled to 200 Hz and partitioned into 15 s epochs for further analysis. Epochs containing artefacts were rejected by generating a histogram of peak-to-peak amplitude for each epoch and rejecting epochs for which this value exceeded the median plus 1 s.d.; between 4% and 8% of epochs were generally rejected using this conservative criterion. Artefact free LFPs were used for all further analysis. Power spectra were calculated for each epoch by FFT and occasional 50 Hz line noise was removed by multitaper filtering. The oscillations are grouped into bands based on their center frequencies: delta (1–5 Hz), theta (5–10 Hz), beta (20–30 Hz) and

gamma (31–80 Hz) and power in each band was calculated by integrating spectral amplitude values.

Decoding behavioral states from LFPs: The purpose of this analysis was to determine how well the BF and VC could classify the behavioral state by using only the spectral power in pairs of frequency bands. With 80% of the epochs corresponding to each behavioral state, we constructed a classifier based on Mahalanobis distance and we then estimated a 2-D state-space decision surface to determine the best behavioral state classification for the testing data (remaining 20% of data). Mahalanobis distance measure makes use of both mean and covariance of each of the three behaviors in the training data set to use as the class prototype for the classifier distance measure. It is preferable to Euclidian distance in cases where variance is non-spherical, as is evidently the case for our data. The isolines in Fig. 3a represent data with the same Mahalanobis distance from the class center for each of the classes. Cross-validation was repeated 100 times with randomized assignment of training and test data, allowing the estimation of confidence intervals. To examine effects of integration time on classification performance, we split each epoch into either 3 five second sub-epochs or 5 three second sub-epochs, and repeated the above procedure.

Coherence and Granger causality spectral analyses: To study connectivity and directional influences between BF and VC, coherence and Granger causality spectral analyses were performed by using the BSMART toolbox (Cui et al., 2008). After data normalizing and detrending, we fitted an autoregressive model (AR) to the time series. Based on the Akaike Information criterion test, we selected a model order number of 15. We also explored other model orders between 5 and 40 time points and found generally similar results. Coherence and Granger causality spectral analyses (0–80 Hz) were conducted using a bivariate model comparing BF and VC time series with a 15 s epoch duration. We conducted statistical comparison averaged across pairs of recording sites using paired t-tests and repeated-measures ANOVAs (SPSS) in frequency ranges of interest (θ: 5–10 Hz; β: 15–20 Hz; γ: 50–70 Hz).

Cross-frequency coupling: We first localized all negative peaks of the δ frequency (1–3 Hz bandpass filtered visual cortical LFP signal) during SWS epochs. We then extracted the corresponding spectral power (10–80 Hz) in a time window around this negative peak (±3 s) using Morlet wavelet analysis (Cohen, 2014). The number of wavelet cycles was adjusted between 3 and 10 cycles by logarithmic function of 40 steps for this frequency range. Power values for every time window were baseline corrected and transformed to decibels (dB) by the averaged baseline interval of −2.9 to −1.9 s before each peak. The mean of these baseline corrected time windows was then plotted for a ±1.5 s window centered on the negative delta peak.

To quantify delta-gamma coupling, we first extracted the amplitude time series at 60 Hz and the phase angle time series at 2 Hz using Morlet wavelet analysis. Subsequently we computed the mean gamma amplitude corresponding to delta phase angle intervals. The modulation strength was determined as the difference between the maximal and the minimal mean amplitude phase bins. In polar plots, the vectors describe modulation strength values and the preferred phase angles (phase bin of the maximal mean amplitude).

3. Results

We have recorded bilateral local field potential (LFP) activity from VC and the nucleus basalis of the BF in eight animals (see Fig. 1a). Electrode and target positions were verified by analysis of Nissl stained sections for relevant regions of the BF and the cortex (see Fig. 1b). Continuous LFP recordings were made during periods lasting about six hours while animals were in their home cage, which included extended periods of wakefulness (WAKE) as well as rapid eye movement (REM) and slow wave sleep (SWS). Based on VC LFP, movement sensor signals and video analysis, the behavioral state was determined manually for epochs of 15 s duration using standard procedures (see methods). A typical movement sensor signal and LFP recording is shown in Fig. 1c, which includes four periods of wakefulness, flanking sleep periods that contained multiple transitions between REM and SWS.

3.1. Spectral BF LFP characteristics during wakefulness, REM and SWS

We first characterized the spectral content of the LFPs in both target locations (see Fig. 2a for a typical single LFP recording). In both BF and VC, we observed delta activity during SWS as well as theta activity during REM and wakefulness. LFP activity at these low frequencies is subject to potential contamination by volume conduction, such as for example from the hippocampus (Buzsáki, 2002; Sirota et al., 2008). We therefore do not proceed to perform a detailed analysis of these effects here, but show the spectra for illustrative purposes only. In the gamma band, we observed broad enhancement in VC during both wakefulness and REM compared to SWS, as well as moderately enhanced activity during wakefulness compared to REM (one-way ANOVA with posthoc tests: $P < 0.01$), consistent with previous findings (Cavelli et al., 2015). In BF, gamma activity displayed clear peaks during all three behavioral states (see Fig. 2b). Gamma power was elevated during wakefulness compared to both sleep states (by 73% and 74% for REM and SWS respectively, one-way ANOVA with posthoc tests, $P < 0.01$) whereas there was no difference in gamma power between REM and SWS (one-way ANOVA with posthoc tests, $P > 0.1$). Gamma peak frequency differed significantly between all three behavioral states (peak γ SWS: 60 Hz, REM: 58 Hz, WAKE: 53 Hz, one-way ANOVA: $P < 0.01$). Gamma activity was thus modulated qualitatively differently in BF and VC: In VC, gamma power was similar during wakefulness and REM, whereas in BF gamma power was similar for SWS and REM. We also observed that elevated beta activity was present alongside the gamma oscillations in BF during wakefulness (62% and 55% enhancement over REM and SWS respectively, one-way ANOVA: $P < 0.01$). Beta activation was less robust than gamma, but clear spectral peaks were observable in 8 out of 14 recordings (peak β: 26 Hz).

A pertinent issue related to the BF gamma oscillations is to what extent these are generated by local networks close to the recording electrode. We were able to address this question by recording action potentials and LFPs simultaneously using a tethered recording system (see methods) in a number of animals ($n = 4$). These recordings revealed that unit activity was strongly dependent on the phase of the gamma cycle for the analyzed units (Hodges-Ajne test with Bonferroni correction $p < 0.01$). This is demonstrated by the polar plots of action potential timing as a function of gamma phase for two example units shown in Fig. 3a. Inter-spike interval distributions that peak around 20–25 ms, as well as spike-triggered averages of the LFPs showing robust gamma oscillations provide additional confirmation of a close coupling of the BF gamma oscillations to local spiking activity (Fig. 3b and c).

3.2. Single trial decoding of behavioral state using BF gamma activity

Given the previously unrecognized prominent gamma activity in BF, we were interested to examine how closely it was linked to behavioral state on single trials based on 15 s duration epochs. We therefore performed a classification analysis, in which we fit ellipses to data from each behavioral state in a two-dimensional space with axes corresponding to power in the beta and gamma bands. Results for an example dataset are shown in Fig. 4a,
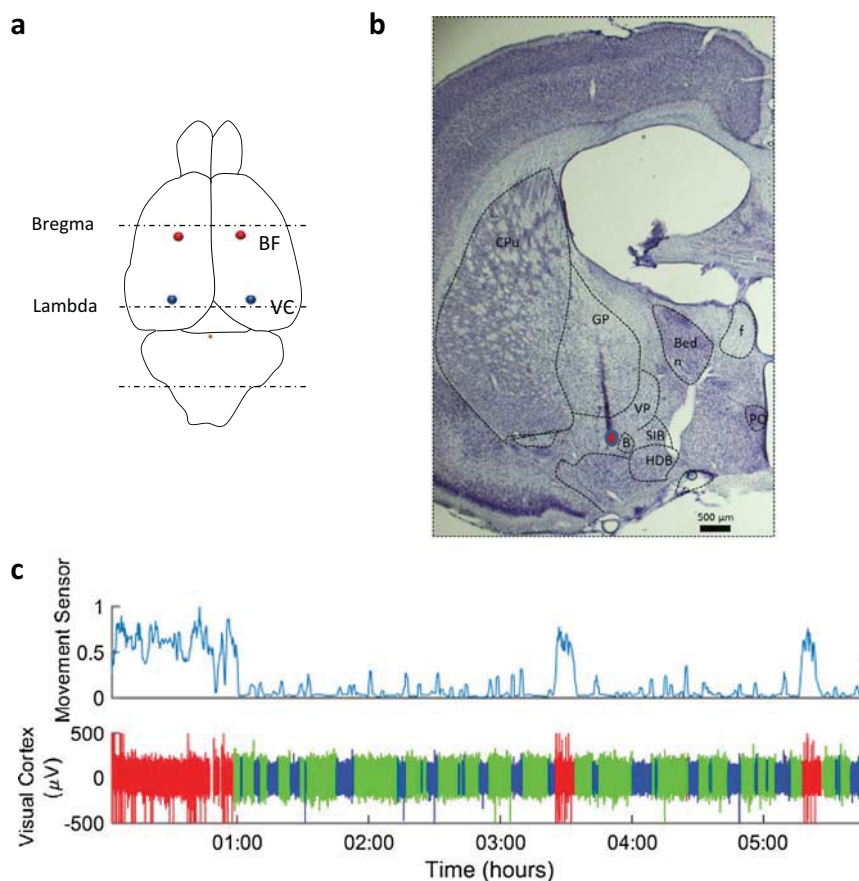
Fig. 1. Recording sites and typical LFP activity. (a) Schematic drawing of the recording sites in basal forebrain (BF) and visual cortex (VC). (b) A representative coronal section showing the tungsten electrode track in the BF. The red dot indicates an example target of the electrode. (c) Movement (top) and LFP (bottom) recorded continuously for 6 h (red WAKE, green SWS, and blue REM).

illustrating clear clustering of activity according to behavioral state. Based on Mahalanobis distance, we computed from these ellipses the decision surface Fig. 4b, which allowed the classification of data not used for constructing the classifier by cross validation. The results shown in Fig. 3c, illustrate that highly accurate decoding of the wakeful behavioral state is possible based on BF and VC LFPs across datasets (n = 16). For example, classification performance of about 85% correct was possible based on BF LFPs, while VC LFPs allowed only 73% correct classification. As illustrated in Fig. 4c, behavioral state decoding performance decreased for shorter epoch durations, but remained above 80% correct in the BF even for the shortest duration tested (3 s epoch). A two-way ANOVA with epoch duration and recording site (BF/VC) confirmed significant main effects of site and duration ($P < 0.01$), as well as a significant interaction ($P < 0.05$). These findings highlight the robust nature of BF gamma activity during wakefulness.

3.3. Functional interactions between BF and VC: coherence

To study functional interactions between BF and VC, we first computed the coherence spectra for each behavioral state based on signals within each brain hemisphere. Peaks in spectral coherence indicate that there is a consistent phase-relationship between signal pairs at that particular frequency across epochs. The coherence spectrum averaged across 14 hemispheres (see Fig. 5a) exhibits clear spectral peaks that are dependent on brain state. In the gamma band, we found clear peaks for WAKE and SWS states but not REM, with peaks occurring at higher frequencies during SWS than WAKE ($P_{\gamma,SWS}$ = 62.5 ± 0.5 Hz, $P_{\gamma,WAKE}$ = 58.96 ± 1.3 Hz; paired t-test: $P < 0.01$). Peak gamma coherence values varied significantly

with brain state, with highest values during WAKE, intermediate during SWS and lowest during REM ($C_{\gamma,WAKE}$ = 0.16 ± 0.02, $C_{\gamma,SWS}$ = 0.13 ± 0.02, $C_{\gamma,REM}$ = 0.06 ± 0.01; one-way ANOVA with posthoc tests: $P < 0.05$). In the beta band, we observed a peak in coherence at around 18 Hz exclusive to the WAKE state ($P_{\beta,WAKE}$ = 18.5 ± 0.3 Hz). Coherence at this frequency was higher in WAKE than in the two sleep states ($C_{\beta,WAKE}$ = 0.07 ± 0.01 Hz, $C_{\beta,SWS}$ = 0.01 ± 0.001 Hz; $C_{\beta,REM}$ = 0.01 ± 0.002 Hz one-way ANOVA with posthoc tests: $P < 0.001$). Our bilateral recordings allow us to compare functional coupling within a hemisphere to corresponding values between hemispheres, allowing us to distinguish more global, bilateral oscillatory coupling from more specific modulations that occur within brain hemispheres. For gamma oscillations, we found significantly greater coupling within than across hemispheres for the WAKE state (see Fig. 5b), and the same was also true for gamma during SWS ($C_{\gamma,SWS, within}$ = 0.13 ± 0.02, $C_{\gamma,SWS, across}$ = 0.04 ± 0.01; paired t-test: $P < 0.005$) (see Fig. 5c). Furthermore, beta oscillations were marginal-significantly more coherent within than across hemispheres ($C_{\beta,WAKE, within}$ = 0.07 ± 0.01, $C_{\beta,WAKE, across}$ = 0.05 ± 0.01; paired t-test: $P = 0.065$). Taken together, this suggests that beta and gamma coherence between BF and VC exhibited specificity within each hemisphere, which would be expected based on the connectivity between the two brain regions that tends to be hemisphere-specific.

3.4. Functional interactions between BF and VC: Granger causality

To further characterize the functional interactions between BF and VC, we used Granger causality analyses that allow a quantifi-
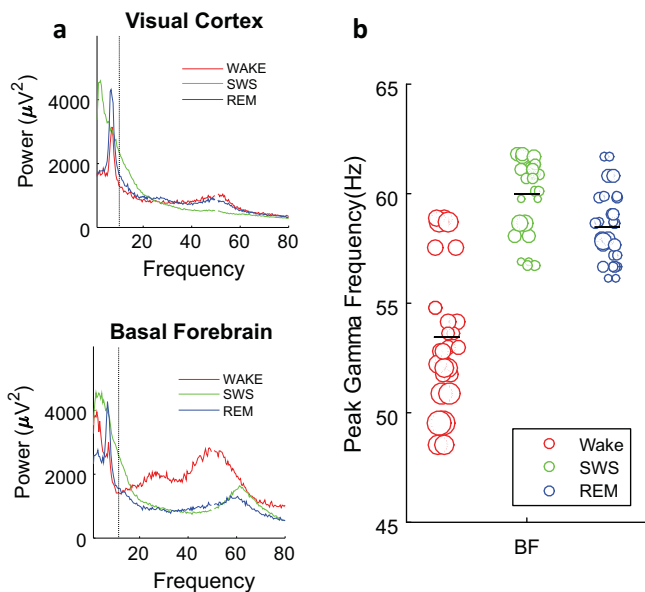
Fig. 2. Spectral characteristics of LFP activity in VC and BF depend on behavioral state. (a) PSD during different behavioral states in a representative animal. In VC, gamma activity was elevated during WAKE and REM compared to SWS. In BF, very pronounced beta and gamma activity occurred during WAKE state, with additional clear gamma peaks of lower amplitude in SWS and REM. Spectral content below 10 Hz is subject to potential contamination by volume conduction and is shown for illustrative purposes only. (b) Peak gamma power in BF was greater in WAKE compared to SWS and REM (diameter of symbols denotes power). In contrast, peak gamma frequency was lower for WAKE (53 Hz) as compared to SWS (60 Hz) and REM (58 Hz).

cation of directional influences of one brain area on another. Thus, a peak in the Granger spectrum indicates that neural activity fluctuations at a given frequency in a target area at time $\tau = \tau_0$ can be predicted based on corresponding values in a source area at times $\tau < \tau_0$. Comparing Granger causality values in both directions, i.e. BF → VC and VC → BF, can provide information about direction and magnitude of net influence during interactions between the two brain areas. The Granger spectra are shown for both directions

in Fig. 6a. In the gamma band, there were pronounced peaks only in the BF → VC direction during WAKE and SWS states. While peak Granger causality values were similar during WAKE and SWS (0.05 ± 0.01 and 0.06 ± 0.01 respectively; paired t-test: $P > 0.1$), gamma oscillations were of higher frequency in SWS than in WAKE state (62.4 ± 0.9 Hz and 55.6 ± 1.6 Hz; paired t-test: $P < 0.001$). Gamma band Granger spectra revealed directionality of functional interactions between BF and VC, which were already apparent in the coherence spectra. By contrast, the beta enhancement observed in the coherence spectra was not apparent in the Granger spectra in either direction. Several potential explanations, including common input affecting signals at both electrodes or volume-conducted noise (Whitmore and Lin, 2016), may account for this finding. Another possibility is that because BF beta tends to occur in short bursts during exploratory behavior (Quinn et al., 2010), it may be less easily detected by Granger causality analyses than more sustained activations. In terms of differences between inter- and intrahemispheric effects, Granger spectra were highly similar to coherence spectra, such that Granger predictions in the gamma band were larger within hemispheres for WAKE (see Fig. 6b) and SWS (two-way ANOVAs with $P < 0.01$).

Granger predictions are not dependent on signal amplitude; they are invariant to multiplicative scaling of source as well as target signals. We nevertheless observed that Granger predictions appeared to be systematically related to frequency band power in a manner that depended on brain state. This is illustrated in Fig. 6c, which plots the source power against Granger prediction for two example cases. In the gamma band, Granger causality and source power modulation both increased from REM to WAKE state, although Granger causality was less strongly enhanced (about 2.5-fold) than source power (Δpower: +72%, ΔGranger: 189%, t-test: $P < 0.01$). Comparing SWS and REM sleep states revealed that Granger predictions can also occur in the absence of source power modulation. Here, power was similar between the two brain states (+0%), whereas Granger predictions were strongly enhanced for SWS over REM (+248%, paired t-test: $P < 0.01$). These analyses demonstrate that Granger causality modulations can be accompanied by source power modulations, but can also occur in their absence.
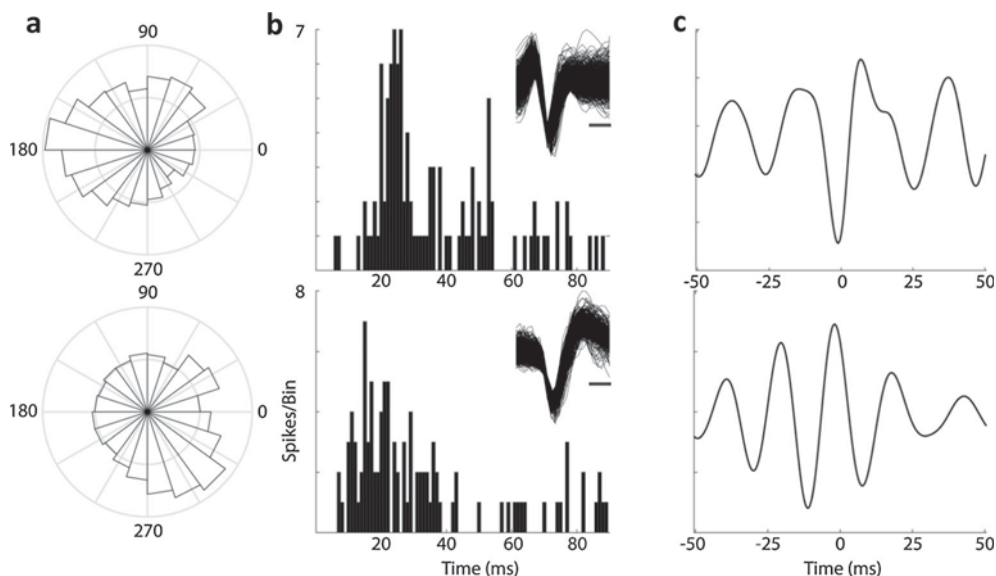

Fig. 3. BF Spiking activity entrained to gamma oscillations. (a) Polar plots of spiking activity as a function of gamma oscillation phase for two example BF units reveal robust entrainment of action potential timing to the gamma oscillation. (b) Inter-spike-interval (ISI) histograms for the example units exhibit peaks at 20–25 ms consistent with gamma oscillation timing. (c) The spike-triggered-average (STA) exhibits robust oscillations, providing further evidence for local generation of gamma oscillations within BF networks.
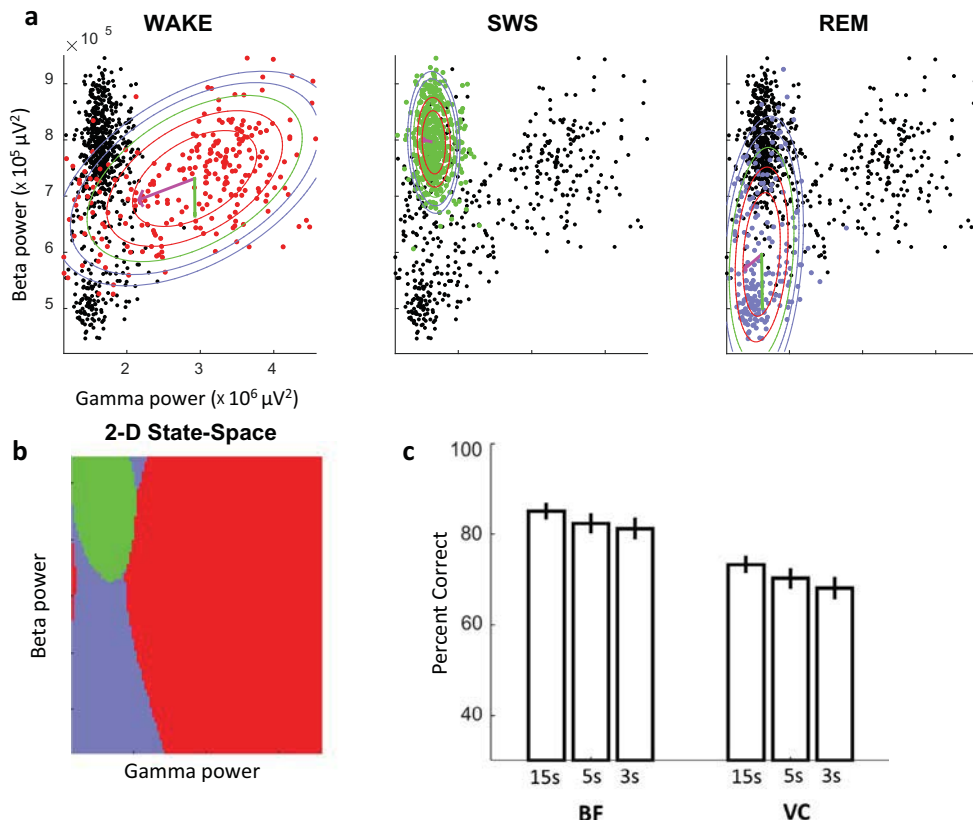
Fig. 4. Behavioral state classification based on Mahalanobis distance classifier. (a) We trained a classifier on a random 80% of neural data epochs (15 s duration) from each behavioral state using beta and gamma frequency power, where the colored dots correspond to that data belonging to each state. (b) A 2-D state-space with a decision surface was generated based on Mahalanobis distance, allowing classification of the remaining 20% of data epochs. (c) Example classification performance for the WAKE state decoded from BF and VC for epoch durations of 3, 5 and 15 s. Note the higher accuracy of decoding performance based on BF data, as well as the dependence on epoch duration.
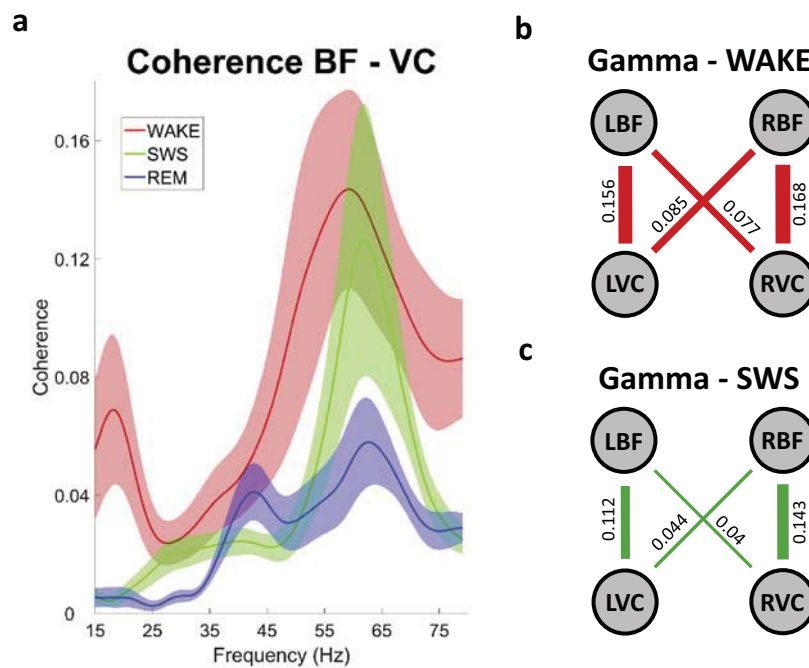
Fig. 5. Coherence spectral analyses of BF and VC. (a) Group mean coherence spectra with shaded areas reflecting 95% confidence intervals. Coherence between VC and BF exhibits gamma peaks during WAKE and SWS compared to REM, and a beta frequency peak during WAKE only. (b) Gamma coherence during WAKE and SWS was greater within than across hemispheres consistent with hemisphere-specific regulation.

6
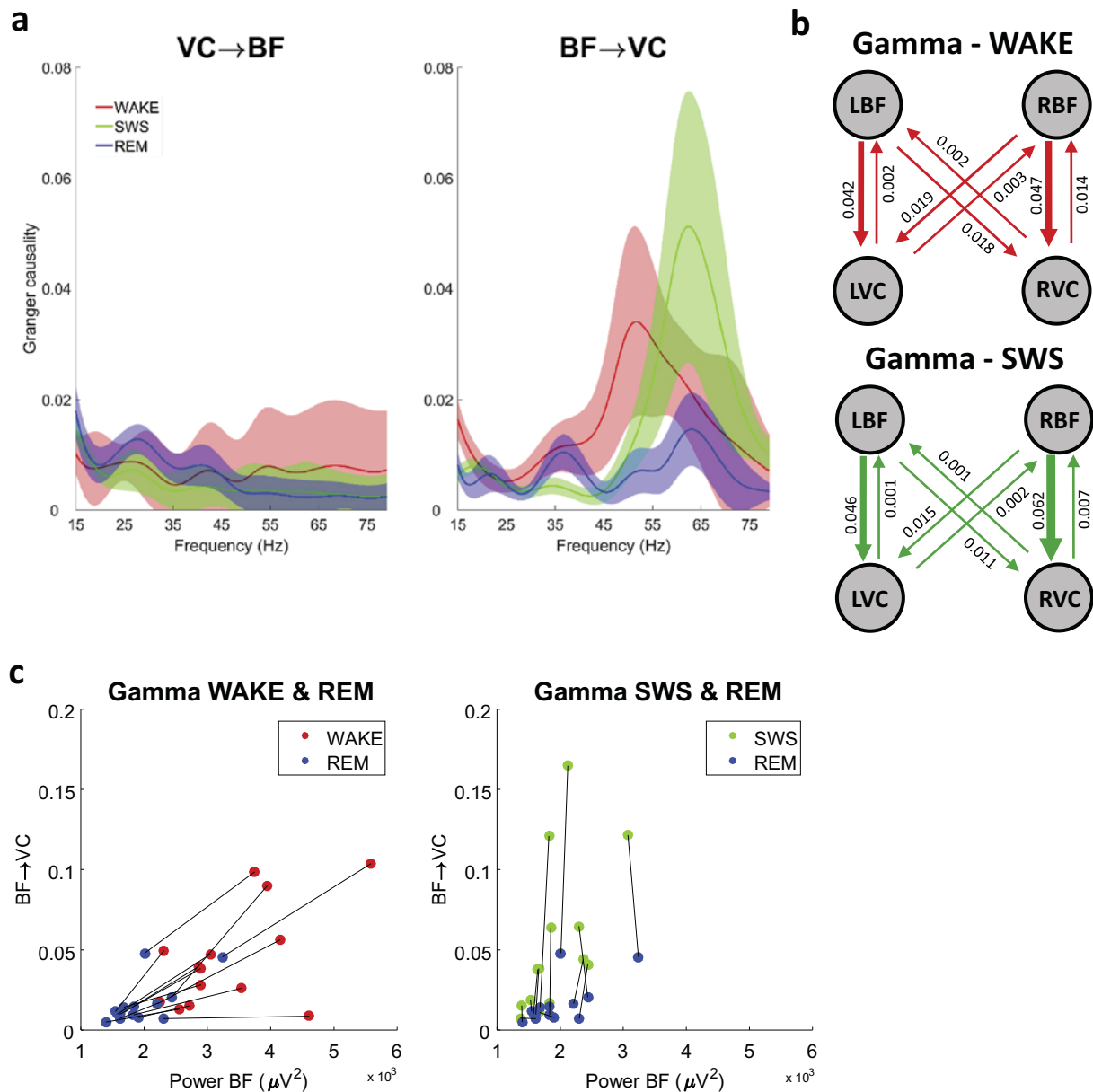
Fig. 6. Granger causality spectral analyses of BF and VC. (a) Group mean Granger causality spectra are shown for predictions directed from VC to BF (left panel) and BF to VC (right panel) during different behavioral states, shaded areas correspond to 95% confidence intervals. Granger causality in the gamma band BF → VC was pronounced during WAKE and SWS, while being largely absent in the VC → BF direction as well as during REM. (b) Granger causality path diagrams summarize group averaged Granger causality peak values for gamma during WAKE and SWS, where arrow thickness denotes prediction strength. (c) Scatter plots illustrate the diversity in the relationship between Granger predictions and source LFP power peaks. The left panel shows that between REM and WAKE states, both Granger predictions and source LFP power were increased, whereas Granger predictions were increased in absence of LFP source power changes between SWS and REM (right panel).

3.5. Cross frequency delta-gamma coupling in VC

The robust SWS gamma band BF-VC coherence and BF → VC Granger prediction raises the question what the function of this long-range coupling might be, particularly since there was little in terms of gamma power during SWS in VC. Given that delta oscillations dominate cortical potentials during SWS, we first asked whether there was a systematic relationship between VC gamma power and the phase of VC delta oscillations. To achieve this, we plotted LFP power between 10 and 80 Hz aligned to the trough of the delta oscillation. The results are shown in Fig. 7a for a typical recording session, illustrating robust modulations of LFP gamma power that were phase-locked to the delta oscillation (see methods). The gamma power distribution for two delta cycles is shown

in Fig. 7b, illustrating the relationship of VC gamma power to the delta oscillation phase. A preferred phase of 230° is apparent for this example dataset. To examine delta-gamma coupling across the population, we estimated the magnitude and preferred phase for each recording session. The results are summarized in Fig. 7c (left panel), showing robust locking of gamma power to delta phase across sessions with a phase preference typically between the peak and the downward slope of the LFP. Each vector represents magnitude and preferred direction of delta-gamma coupling within VC. For comparison, we repeated this same analysis for the WAKE state and REM state (Fig. 7c, center panels), and it is apparent that delta-gamma coupling appears weaker in these states compared to SWS. To quantify these effects, we estimated the resultant vector for each behavioral state, and then computed the
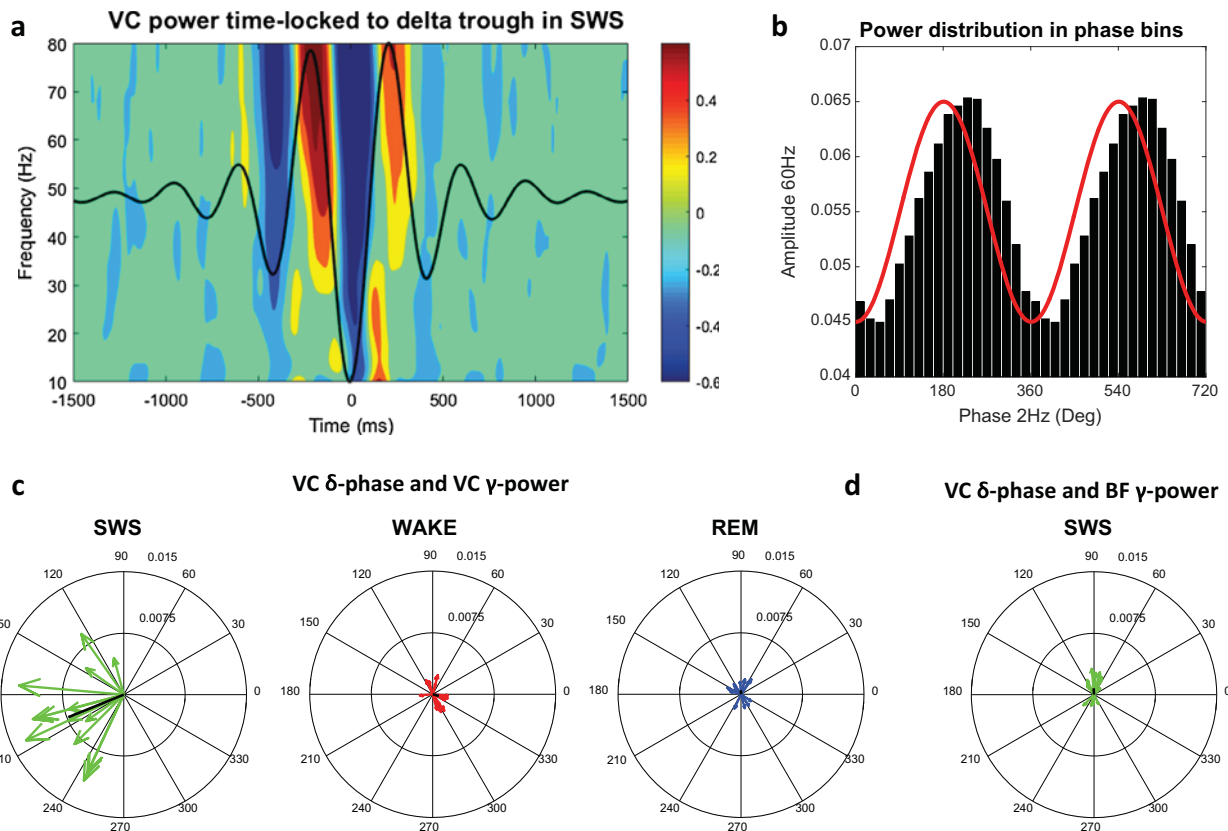
Fig. 7. Delta-gamma phase-amplitude coupling in the VC during slow wave sleep. (a) Time frequency plot shows mean amplitude distribution time-locked to the negative peaks in the delta oscillation. The delta filtered peak-locked averaged signal is plotted as a black line and highlights enhanced gamma amplitude around the peaks of delta oscillations. (b) Gamma amplitude at 60 Hz is plotted as a function of delta phase, with gamma amplitude values binned into eighteen 20° intervals. The red line represents the corresponding delta wave cycle at 2 Hz and shows maximal gamma amplitude at a phase of 230°. (c) Polar plots of vector denoting magnitude and preferred direction of delta-gamma coupling within VC (*n* = 14 datasets) for each behavioral state, revealing robust coupling in SWS compared to REM and WAKE. The black line denotes the resultant vector for each behavioral state. (d) Polar plot showing that BF gamma power was not coupled strongly to cortical delta oscillation phase during SWS.

magnitude of the projection for each dataset onto this resultant. The magnitude of the projections were larger for SWS than both REM and WAKE (one-way ANOVA, $P < 0.001$), with no differences between REM and WAKE (one-way ANOVA, $P > 0.1$). Having confirmed the well-known interplay between cortical gamma and delta waves during SWS, we proceeded to examine if BF gamma power was also coupled to cortical delta waves. Using the same analyses as above, we showed that there was no such relationship present in our data (see Fig. 7d). Indeed, the magnitude of coupling between VC delta and BF gamma was far lower than the coupling observed within VC as analyzed above (paired *t*-test based on vector projections on resultant direction, $P < 0.001$). These analyses suggest that although there appears to be a directed interaction between BF and VC in the gamma range during SWS, this interaction is unrelated to the generation of cortical delta waves.

4. Discussion

We have described interactions between the BF and VC and their directionality based on LFP recordings during wakefulness (WAKE), rapid-eye movement (REM) and slow-wave sleep (SWS).

Our results are based on LFP recordings, whose biophysical origin continues to be debated (Sirota et al., 2008; Berens et al., 2008; Katzner et al., 2009; Xing et al., 2009; Kajikawa and Schroeder, 2011; Rainer, 2014). In our view, the LFP is an aggregate signal that is influenced by both super and subthreshold synaptic activations due to local recurrent processing, inputs from distant axonal sources (Nielsen et al., 2006; Rainer, 2008), as well as ephaptic

coupling (Anastassiou et al., 2011) and non-synaptic sources due to volume-transmitted neuromodulators or gap junctions. In addition, because electric fields propagate in the brain, LFP recordings may also reflect propagated signals from nearby sources, a process that is known as volume conduction, which is particularly relevant when strong generators for the observed oscillatory phenomena are known to exist. Convergent evidence suggests that higher frequency oscillations in the beta and gamma range tend to reflect local synchronized firing and are not passively propagated over large distances (Steriade and Amzica, 1996; Buzsáki and Wang, 2012; Buzsáki et al., 2012; Welle and Contreras, 2016). Low frequency LFP modulations in delta, theta and alpha bands however need to be interpreted with particular caution, given the robust, large amplitude, and highly synchronized theta oscillations that are present in the hippocampus that have been shown to affect cortical LFP recordings particularly in the rat where these structures are in close proximity (Buzsáki, 2002; Sirota et al., 2008). For this reason, we focus our analyses and interpretation largely on beta and gamma band activity here.

We observed broad gamma band peaks in VC during WAKE and REM states but not during SWS as expected based on previous literature (Buzsáki and Wang, 2012). BF exhibited a very prominent gamma-band activity peak during WAKE, as well as robust gamma peaks during SWS and REM sleep. The peak gamma frequency differed between all three states, indicating that gamma is differentially regulated depending on behavioral state in BF and suggesting that gamma might be generated by at least partially non-overlapping neural populations during WAKE, REM and SWS.

The high gamma power in BF compared to cortex is unexpected, given that a regular geometric arrangement of dendrites is thought to be one of the most important factors contributing to LFP amplitude (Buzsáki et al., 2012) and that such an arrangement is certainly less prevalent in BF than in the cortex. One factor contributing to the prominent BF gamma oscillations may be the presence of gap junctions, which have been reported in BF populations (McKenna et al., 2013) and which can synchronize temporal neural activity (Gibson et al., 1999; Deans et al., 2001), thus enhancing the overall LFP amplitude. Certain membrane characteristics, by which neurons can generate intrinsic gamma oscillations (Garcia-Rill et al., 2014) without the need of excitatory-inhibitory coupling, could also be at work in BF to generate the observed large gamma power. Regardless of the mechanism of generation, BF LFPs and in particular their gamma components are highly sensitive to brain state, and in fact allow more accurate decoding of the WAKE state than visual cortical LFPs. Robust gamma oscillations have previously been demonstrated in the ventral striatum, raising the possibility that the gamma signals recorded in the BF may be dominated by components that have propagated to the BF from this brain region. We consider that this is unlikely for several reasons, including poor coherence of gamma within the ventral striatum (Kalenscher et al., 2010; Malhotra et al., 2015), completely different spectral signatures related to SWS and REM states between the two structures (Hunt et al., 2009), reversed cortical-subcortical information flow direction during wakefulness (Horschig et al., 2015) and coupling of gamma oscillations to local spiking activity as demonstrated in the present study. Nevertheless, further systematic studies are needed to unravel how gamma oscillations in the basal forebrain and nearby brain structures including the ventral striatum (van der Meer and Redish, 2009; Berke, 2009) are regulated.

Functional interactions between BF and VC in the gamma band were strongly directional. In the VC → BF direction there was virtually no directed interaction, whereas there was robust evidence for Granger causality in the BF → VC direction during WAKE and SWS states. Our observation of a robust gamma band Granger prediction from BF to VC is related to previous work showing that manipulations resulting in BF activation produce gamma oscillations in cortex (Bhattacharyya et al., 2013; Kim et al., 2015), which are thought to be mediated mainly by GABAergic BF corticopetal projections (Kim et al., 2015; Zant et al., 2016). Indeed, both cholinergic and particular classes of GABAergic neurons, termed "W-max" and "WP-max", are known to be activated during wakefulness (Hassani et al., 2009). Our results suggest that the network activity of this wake-promoting BF corticopetal system produces high amplitude gamma oscillatory activity at a – compared to sleep states – relatively low peak frequency. During SWS, we also observed a robust gamma-band Granger prediction in the BF → VC direction. We consider this directional influence is to be mediated by a network that includes GABAergic "S-max" BF neurons, which have been shown to be most highly active during SWS and are the major component of the BF sleep promoting system (Hassani et al., 2009). Interestingly, unit activity of BF "S-max" and related cells has been linked to cortical delta waves that dominate the cortical EEG or LFP spectrum during SWS (Manns et al., 2000b; Lee et al., 2004), although this does not appear to be the case for all "S-max" neurons (Hassani et al., 2009). Our findings suggest that BF gamma during SWS in fact is not functionally related to VC delta waves, as is the case for VC gamma. The nature of the BF → VC gamma functional interaction remains a subject for future investigations. BF gamma oscillations during REM sleep are of interest, since in terms of gamma power they were similar to SWS, but showed neither coherence nor Granger prediction with VC. We suggest that REM BF gamma is mediated mainly by "P-max" as well as "WP-max" GABAergic neurons, given that these are fast-spiking neurons that are most active during REM sleep. Consistent with our findings, the "P-max" GABAergic BF population does not in fact project to cortex, but instead targets the hypothalamus (Gritti et al., 1994) and brainstem structures (Semba et al., 1989) including the medulla that has recently been linked to REM sleep initiation (Weber et al., 2015).

Our findings recapitulate major aspects of the BF-cortex projection systems during WAKE, SWS and REM states, and link the corresponding BF projection systems to specific oscillation frequencies in the gamma band. We suggest that electrical or optogenetic activation of BF networks may be most effective, when it occurs at the frequency that corresponds to the peak of the endogenously generated gamma activity in the respective behavioral state. The Granger analyses presented here produced highly reliable results that captured many aspects of BF circuits that have been established in prior studies. Granger causality analyses appear to be particularly useful for unraveling directional influences of deep brain nuclei on the cortex consistent with other recent findings (Horschig et al., 2015; Sawada et al., 2015), because these structures are well separated in space and coupled by long range projections. We suggest that our approach may thus generate useful results also in other neuromodulatory systems where these analyses have not been conducted so far.

Acknowledgements

References

Anaclet, C., Pedersen, N.P., Ferrari, L.L., Venner, A., Bass, C.E., Arrigoni, E., Fuller, P.M., 2015. Basal forebrain control of wakefulness and cortical rhythms. Nat. Commun. 6, 8744.

Anastassiou, C.A., Perin, R., Markram, H., Koch, C., 2011. Ephaptic coupling of cortical neurons. Nat. Neurosci. 14, 217–223.

Berens, P., Keliris, G.A., Ecker, A.S., Logothetis, N.K., Tolias, A.S., 2008. Feature selectivity of the gamma-band of the local field potential in primate primary visual cortex. Front. Neurosci. 2, 199–207.

Berke, J.D., 2009. Fast oscillations in cortical-striatal networks switch frequency following rewarding events and stimulant drugs. Eur. J. Neurosci. 30, 848–859.

Berntson, G.G., Shafi, R., Sarter, M., 2002. Specific contributions of the basal forebrain corticopetal cholinergic system to electroencephalographic activity and sleep/waking behaviour. Eur. J. Neurosci. 16, 2453–2461.

Bhattacharyya, A., Bießmann, F., Veit, J., Kretz, R., Rainer, G., 2012. Functional and laminar dissociations between muscarinic and nicotinic cholinergic neuromodulation in the tree shrew primary visual cortex. Eur. J. Neurosci. 35, 1270–1280.

Bhattacharyya, A., Veit, J., Kretz, R., Bondar, I., Rainer, G., 2013. Basal forebrain activation controls contrast sensitivity in primary visual cortex. BMC Neurosci. 14, 55.

Bressler, S.L., Seth, A.K., 2011. Wiener-Granger causality: a well established methodology. Neuroimage 58, 323–329.

Brovelli, A., Ding, M., Ledberg, A., Chen, Y., Nakamura, R., Bressler, S.L., 2004. Beta oscillations in a large-scale sensorimotor cortical network: directional influences revealed by Granger causality. Proc. Natl. Acad. Sci. 101, 9849–9854.

Buzsáki, G., 2002. Theta oscillations in the hippocampus. Neuron 33, 325–340.

Buzsáki, G., Anastassiou, C.A., Koch, C., 2012. The origin of extracellular fields and currents—EEG, ECoG, LFP and spikes. Nat. Rev. Neurosci. 13, 407–420.

Buzsaki, G., Bickford, R.G., Ponomareff, G., Thal, L.J., Mandel, R., Gage, F.H., 1988. Nucleus basalis and thalamic control of neocortical activity in the freely moving rat. J. Neurosci. 8, 4007–4026.

Buzsáki, G., Wang, X.-J., 2012. Mechanisms of gamma oscillations. Annu. Rev. Neurosci. 35, 203–225.

Cape, E.G., Jones, B.E., 1998. Differential modulation of high-frequency gamma-electroencephalogram activity and sleep-wake state by noradrenaline and serotonin microinjections into the region of cholinergic basalis neurons. J. Neurosci. 18, 2653–2666.

Cape, E.G., Jones, B.E., 2000. Effects of glutamate agonist versus procaine microinjections into the basal forebrain cholinergic cell area upon gamma and theta EEG activity and sleep-wake state. Eur. J. Neurosci. 12, 2166–2184.

Cape, E.G., Manns, I.D., Alonso, A., Beaudet, A., Jones, B.E., 2000. Neurotensin-induced bursting of cholinergic basal forebrain neurons promotes gamma and theta cortical activity together with waking and paradoxical sleep. J. Neurosci. 20, 8452–8461.

Cavelli, M., Castro, S., Schwarzkopf, N., Chase, M.H., Falconi, A., Torterolo, P., 2015. Coherent neocortical gamma oscillations decrease during REM sleep in the rat. Behav. Brain Res. 281, 318–325.

Chen, M., Yan, Y., Gong, X., Gilbert, C.D., Liang, H., Li, W., 2014. Incremental integration of global contours through interplay between visual cortical areas. Neuron 82, 682–694.

Cohen, M.X., 2014. Analyzing Neural Time Series Data: Theory and Practice. MIT Press, London.

Cui, J., Xu, L., Bressler, S.L., Ding, M., Liang, H., 2008. BSMART: a Matlab/C toolbox for analysis of multichannel neural time series. Neural Networks 21, 1094–1104.

Deans, M.R., Gibson, J.R., Sellitto, C., Connors, B.W., Paul, D.L., 2001. Synchronous activity of inhibitory networks in neocortex requires electrical synapses containing connexin36. Neuron 31, 477–485.

Duque, A., Balatoni, B., Detari, L., Zaborszky, L., 2000. EEG correlation of the discharge properties of identified neurons in the basal forebrain. J. Neurophysiol. 84, 1627–1635.

Fuller, P., Sherman, D., Pedersen, N.P., Saper, C.B., Lu, J., 2011. Reassessment of the structural basis of the ascending arousal system. J. Comp. Neurol. 519, 933–956.

Garcia-Rill, E., Kezunovic, N., D'Onofrio, S., Luster, B., Hyde, J., Bisagno, V., Urbano, F. J., 2014. Gamma band activity in the RAS-intracellular mechanisms. Exp. Brain Res. 232, 1509–1522.

Gibson, J.R., Beierlein, M., Connors, B.W., 1999. Two networks of electrically coupled inhibitory neurons in neocortex. Nature 402, 75–79.

Gritti, I., Mainville, L., Jones, B.E., 1994. Projections of GABAergic and cholinergic basal forebrain and GABAergic preoptic-anterior hypothalamic neurons to the posterior lateral hypothalamus of the rat. J. Comp. Neurol. 339, 251–268.

Grosmark, A.D., Mizuseki, K., Pastalkova, E., Diba, K., Buzsáki, G., 2012. REM sleep reorganizes hippocampal excitability. Neuron 75, 1001–1007.

Hassani, O.K., Lee, M.G., Henny, P., Jones, B.E., 2009. Discharge profiles of identified GABAergic in comparison to cholinergic and putative glutamatergic basal forebrain neurons across the sleep-wake cycle. J. Neurosci. 29, 11828–11840.

Horschig, J.M., Smolders, R., Bonnefond, M., Schoffelen, J.-M., van den Munckhof, P., Schuurman, P.R., Cools, R., Denys, D., Jensen, O., 2015. Directed communication between nucleus accumbens and neocortex in humans is differentially supported by synchronization in the theta and alpha band. PLoS ONE 10, e0138685.

Hunt, M.J., Matulewicz, P., Gottesmann, C., Kasicki, S., 2009. State-dependent changes in high-frequency oscillations recorded in the rat nucleus accumbens. Neuroscience 164, 380–386.

Jones, B.E., 2003. Arousal systems. Front. Biosci. 8, s438–s451.

Kajikawa, Y., Schroeder, C.E., 2011. How local is the local field potential? Neuron 72, 847–858.

Kalenscher, T., Lansink, C.S., Lankelma, J.V., Pennartz, C.M.A., 2010. Reward-associated gamma oscillations in ventral striatum are regionally differentiated and modulate local firing activity. J. Neurophysiol. 103, 1658–1672.

Kang, D. et al., 2015. Theta-rhythmic drive between medial septum and hippocampus in slow wave sleep and microarousal: a Granger causality analysis. J. Neurophysiol. 114, 2797–2803.

Katzner, S., Nauhaus, I., Benucci, A., Bonin, V., Ringach, D.L., Carandini, M., 2009. Local origin of field potentials in visual cortex. Neuron 61, 35–41.

Kaur, S., Junek, A., Black, M.A., Semba, K., 2008. Effects of ibotenate and 192IgG-saporin lesions of the nucleus basalis magnocellularis/substantia innominata on spontaneous sleep and wake states and on recovery sleep after sleep deprivation in rats. J. Neurosci. 28, 491–504.

Kim, T., Thankachan, S., McKenna, J.T., McNally, J.M., Yang, C., Choi, J.H., Chen, L., Kocsis, B., Deisseroth, K., Strecker, R.E., Basheer, R., Brown, R.E., McCarley, R.W., 2015. Cortically projecting basal forebrain parvalbumin neurons regulate cortical gamma band oscillations. Proc. Natl. Acad. Sci. 112, 3535–3540.

de Lavilléon, G., Lacroix, M.M., Rondi-Reig, L., Benchenane, K., 2015. Explicit memory creation during sleep demonstrates a causal role of place cells in navigation. Nat. Neurosci. 18, 493–495.

Lee, M.G., Hassani, O.K., Alonso, A., Jones, B.E., 2005. Cholinergic basal forebrain neurons burst with theta during waking and paradoxical sleep. J. Neurosci. 25, 4365–4369.

Lee, M.G., Manns, I.D., Alonso, A., Jones, B.E., 2004. Sleep-wake related discharge properties of basal forebrain neurons recorded with micropipettes in head-fixed rats. J. Neurophysiol. 92, 1182–1198.

Lin, S., Brown, R.E., Shuler, M.G.H., Petersen, C.C.H., 2015. Optogenetic dissection of the basal forebrain neuromodulatory control of cortical activation, plasticity and cognition. J. Neurosci. 35, 1–20.

Lin, S.-C., Nicolelis, M.A.L., 2008. Neuronal ensemble bursting in the basal forebrain encodes salience irrespective of valence. Neuron 59, 138–149.

Malhotra, S., Cross, R.W., Zhang, A., van der Meer, M.A.A., 2015. Ventral striatal gamma oscillations are highly variable from trial to trial, and are dominated by behavioural state, and only weakly influenced by outcome value. Eur. J. Neurosci. 42, 2818–2832.

Manns, I.D., Alonso, A., Jones, B.E., 2000a. Discharge properties of juxtacellularly labeled and immunohistochemically identified cholinergic basal forebrain neurons recorded in association with the electroencephalogram in anesthetized rats. J. Neurosci. 20, 1505–1518.

Manns, I.D., Alonso, A., Jones, B.E., 2000b. Discharge profiles of juxtacellularly labeled and immunohistochemically identified GABAergic basal forebrain neurons recorded in association with the electroencephalogram in anesthetized rats. J. Neurosci. 20, 9252–9263.

McKenna, J.T., Yang, C., Franciosi, S., Winston, S., Abarr, K.K., Rigby, M.S., Yanagawa, Y., McCarley, R.W., Brown, R.E., 2013. Distribution and intrinsic membrane properties of basal forebrain GABAergic and parvalbumin neurons in the mouse. J. Comp. Neurol. 521, 1225–1250.

McLin III, D.E., Miasnikov, A.A., Weinberger, N.M., McLin I, D.E., 2002. The effects of electrical stimulation of the nucleus basalis on the electroencephalogram, heart rate, and respiration. Behav. Neurosci. 116, 795–806.

van der Meer, M.A.A., Redish, A.D., 2009. Low and high gamma oscillations in rat ventral striatum have distinct relationships to behavior, reward, and spiking activity on a learned spatial decision task. Front. Integr. Neurosci. 3, 9.

Metherate, R., Cox, C.L., Ashe, J.H., 1992. Cellular bases of neocortical activation: modulation of neural oscillations by the nucleus basalis and endogenous acetylcholine. J. Neurosci. 12, 4701–4711.

Nguyen, D.P., Lin, S.-C., 2014. A frontal cortex event-related potential driven by the basal forebrain. Elife 3, e02148.

Nielsen, K.J., Logothetis, N.K., Rainer, G., 2006. Dissociation between local field potentials and spiking activity in macaque inferior temporal cortex reveals diagnosticity-based encoding of complex objects. J. Neurosci. 26, 9639–9645.

Plomp, G., Quairiaux, C., Kiss, J.Z., Astolfi, L., Michel, C.M., 2014. Dynamic connectivity among cortical layers in local and large-scale sensory processing. Eur. J. Neurosci. 40, 3215–3223.

Quinn, L.K., Nitz, D.A., Chiba, A.A., 2010. Learning-dependent dynamics of beta-frequency oscillations in the basal forebrain of rats. Eur. J. Neurosci. 32, 1507–1515.

Rainer, G., 2008. Localizing cortical computations during visual selection. Neuron 57, 480–481.

Rainer, G., 2014. Local field potential in the visual system. Encycl. Comput. Neurosci., 1534–1540.

Sawada, M., Kato, K., Kunieda, T., Mikuni, N., Miyamoto, S., Onoe, H., Isa, T., Nishimura, Y., 2015. Function of the nucleus accumbens in motor control during recovery after spinal cord injury. Science 350, 98–101.

Semba, K., 2000. Multiple output pathways of the basal forebrain: organization, chemical heterogeneity, and roles in vigilance. Behav. Brain Res. 115, 117–141.

Semba, K., Reiner, P.B., McGeer, E.G., Fibiger, H.C., 1989. Brainstem projecting neurons in the rat basal forebrain: neurochemical, topographical, and physiological distinctions from cortically projecting cholinergic neurons. Brain Res. Bull. 22, 501–509.

Seth, A.K., Barrett, A.B., Barnett, L., 2015. Granger causality analysis in neuroscience and neuroimaging. J. Neurosci. 35, 3293–3297.

Sirota, A., Montgomery, S., Fujisawa, S., Isomura, Y., Zugaro, M., Buzsáki, G., 2008. Entrainment of neocortical neurons and gamma oscillations by the hippocampal theta rhythm. Neuron 60, 683–697.

Steriade, M., Amzica, F., 1996. Intracortical and corticothalamic coherency of fast spontaneous oscillations. Proc. Natl. Acad. Sci. USA 93, 2533–2538.

Szymusiak, R., Alam, N., McGinty, D., 2000. Discharge patterns of neurons in cholinergic regions of the basal forebrain during waking and sleep. Behav. Brain Res. 115, 171–182.

Thomson, E., Lou, J., Sylvester, K., McDonough, A., Tica, S., Nicolelis, M.A., 2014. Basal forebrain dynamics during a tactile discrimination task. J. Neurophysiol. 112, 1179–1191.

Tingley, D., Alexander, A.S., Kolbu, S., de Sa, V.R., Chiba, A.A., Nitz, D.A., 2014. Task-phase-specific dynamics of basal forebrain neuronal ensembles. Front. Syst. Neurosci. 8, 174.

Tingley, D., Alexander, A.S., Quinn, L.K., Chiba, A.A., Nitz, D.A., 2015. Cell assemblies of the basal forebrain. J. Neurosci. 35, 2992–3000.

Tóth, A., Hajnik, T., Zaborszky, L., Detari, L., 2007. Effect of basal forebrain neuropeptide Y administration on sleep and spontaneous behavior in freely moving rats. Brain Res. Bull. 72, 293–301.

Toth, A., Zaborszky, L., Detari, L., 2005. EEG effect of basal forebrain neuropeptide Y administration in urethane anaesthetized rats. Brain Res. Bull. 66, 37–42.

Weber, F., Chung, S., Beier, K.T., Xu, M., Luo, L., Dan, Y., 2015. Control of REM sleep by ventral medulla GABAergic neurons. Nature 526, 435–438.

Welle, C.G., Contreras, D., 2016. Sensory-driven and spontaneous gamma oscillations engage distinct cortical circuitry. J. Neurophysiol. 115, 1821–1835.

Whitmore, N.W., Lin, S.-C., 2016. Unmasking local activity within local field potentials (LFPs) by removing distal electrical signals using independent component analysis. Neuroimage 132, 79–92.

Wilson, D.A. et al., 2010. Sleep-like states modulate functional connectivity in the rat olfactory system. J. Neurophysiol. 104, 3231–3239.

Xing, D., Yeh, C.-I., Shapley, R.M., 2009. Spatial spread of the local field potential and its laminar variation in visual cortex. J. Neurosci. 29, 11540–11549.

Xu, M., Chung, S., Zhang, S., Zhong, P., Ma, C., Chang, W.-C., Weissbourd, B., Sakai, N., Luo, L., Nishino, S., Dan, Y., 2015. Basal forebrain circuit for sleep-wake control. Nat. Neurosci. 18, 1641–1647.

Yang, C., McKenna, J.T., Zant, J.C., Winston, S., Basheer, R., Brown, R.E., 2014. Cholinergic neurons excite cortically Projecting basal forebrain GABAergic neurons. J. Neurosci. 34, 2832–2844.

Zaborszky, L., Duque, A., 2003. Sleep-wake mechanisms and basal forebrain circuitry. Front. Biosci. 8, d1146–d1169.

Zaborszky, L., Pang, K., Somogyi, J., Nadasdy, Z., Kallo, I., 1999. The basal forebrain corticopetal system revisited. In: Ann. NY Acad. Sci., pp. 339–367.

Zant, J.C., Kim, T., Prokai, L., Szarka, S., McNally, J., McKenna, J.T., Shukla, C., Yang, C., Kalinchuk, A.V., McCarley, R.W., Brown, R.E., Basheer, R., 2016. Cholinergic neurons in the basal forebrain promote wakefulness by actions on neighboring non-cholinergic neurons: an opto-dialysis study. J. Neurosci. 36, 2057–2067.